

Accounts

Photodissociation of Small Molecules in the Gas Phase

Masahiro Kawasaki* **and Richard Bersohn†**

Department of Molecular Engineering and Graduate School of Global Environmental Studies, Kyoto University, Kyoto 606-8501

†Department of Chemistry, Columbia University, New York, NY 10027, USA

(Received December 27, 2001)

Our knowledge of the process of photodissociation is built on a foundation of molecular spectroscopy developed since the 1920's. However, modern photodissociation dynamics has been mainly created by the introduction of laser light sources around 1970. This review of molecular photodissociation emphasizes findings based on techniques developed in the past ten–fifteen years. These include measurement of the energy dependence of the branching ratios of the yields of different photodissociation channels and the distribution of velocity and internal states of the fragments. The time scale of the separation of the fragments is shown to vary from the microsecond to the femtosecond regime depending on whether the dissociation is indirect or direct. Multiphoton dissociation can be incoherent or coherent. In the latter case, if two different optical paths can accomplish dissociation, changing the relative phase of the transition matrix elements of the two paths can control the branching ratio of different channels. The branching ratio can also be controlled by aligning the parent molecule in an electric field or by using successive ultraviolet and infrared transitions. The review concludes with some applications of photodissociation to the terrestrial atmosphere and to the generation of reactive radical sources.

Photodissociation is the formation of two (or more) fragments following absorption of light by a molecule.[1–6] This process has been extensively studied indirectly. The indirect method is to irradiate a gas for a certain period of time and then to analyze the products. However, these stable products may or may not be the fragments produced by photodissociation. The radicals are quickly transformed into other species and even the stable molecules may result from secondary reactions, in particular, that of radical recombination.

Detection of the primary fragments of dissociation requires, therefore, detection on a time scale short compared to the mean time between reactive collisions. The ratio of these two times can be minimized by minimizing the time between formation and detection or by maximizing the time between collisions. The oldest and simplest method is to use photon energies sufficiently high that one of the fragments is electronically excited as expressed by the equation

$$AB + \hbar\omega \rightarrow A^* + B \quad (1)$$

where A^* is electronically excited and fluorescent. The time scale for observation is then limited to pressures so low that the fluorescence lifetime (typically nanoseconds) is short compared to the mean time between collisions. The first experiments of this type, reported in the 1930's were on the alkali halide molecules in which A^* was an alkali atom in an excited state.[7] Later examples include the generation of $OH(A^2\Sigma)$ from H_2O,[8] $CN(B^2\Sigma)$ from ICN,[9] $NH(c^1\Pi)$ from NH_3 and RNH_2,.[10–11] and $I_2(D'^3\Pi_{2g})$ from CH_2I_2.[12] Because the rate of internal conversion increases rapidly with the number of atoms in the molecule fluorescence is limited to small fragments. Indeed the fluorescent fragments so far reported with more than two atoms are NO_2 from N_2O_4,[13] NCO from HNCO,[14] CHF from $CHFCl_2$ and $CHFBr_2$[15], and CH_3S from $(CH_3S)_2$.[16] Fluorescence is also inhibited by increasing the number of atoms in a parent precursor molecule. For example, fluorescence is seen from CN radicals dissociated from HCN but is not observed for CN dissociated from CH_3CN.[17] Production of the electronically excited photofragments requires high photon energies in the vacuum ultraviolet region (VUV) and relatively small molecules in size. Otherwise, quantum yields of emission are zero or very low due to rapid energy dissipation paths. Thus, the detection of emission is a relatively simple way to study photodissociation dynamics, but is limited in its applicability.

Infrared fluorescence from vibrationally excited levels would appear to be a very general detection method. However, because typical IR radiative lifetimes are long compared to mean free times between collisions, this is a difficult experiment. In other words vibrational relaxation rates are often faster than IR emission rates. The time-resolved emission from various levels of ν_4 of CH_3 dissociated from CH_3I and NO

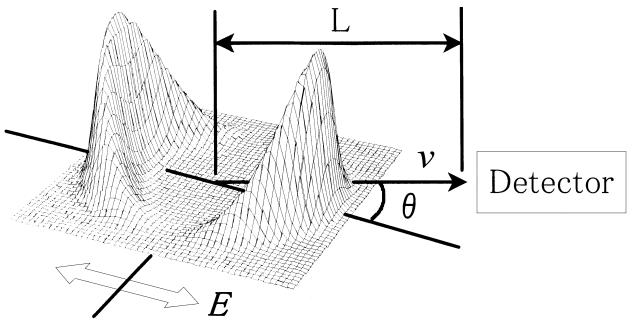

Fig. 1. The velocity $\boldsymbol{v}$ distribution of photofragments is shown by the hatched area for the parallel electronic transition where the angular distribution is defined by $\beta = 2$ in Eq. 5. θ is the angle between the fragment velocity and the electric vector of dissociation light. Photodissociation into fragments occurs at the center. Time-of-flight measurement is performed with a detector fixed L away from the photodissociation point. The translational distribution is obtained by Eq. 4 using a flight length L. The photofragment imaging technique with a combination of multichannel plates and a CCD camera makes possible for us to see this velocity distribution image.

from NO_2 are successful examples.[18–20]

A far more general way to detect a fragment is to use one laser to dissociate a molecule and a second laser to probe the fragment just a short time after its formation. These nascent fragments that are detected at such short times and at such low pressures that they have undergone only a few or even no collisions, are clearly primary products of photodissociation. What is actually detected is not the fragment but fluorescence that is characteristic of the fragment. Ions can be formed by the absorption of a single VUV photon or a series of photons, usually resonant with a particular molecular energy level. A desirable check is the measurement of the mass of the ion by a mass spectrometer.

An alternate way of preserving the pristine character of the fragment is to photolyze a molecular beam of parent molecules in a very high vacuum chamber and then detect the fragments in a second chamber some distance away.[21–25] Schematics of the time-of flight measurement are shown in Fig. 1. The fragments are ionized using either accelerated electrons or photons, and the ions are detected by use of an electron multiplier or a phosphor behind it. This is the most general way of detecting molecular fragments.

1. Photodissociation Dynamics

1.1. Photon Energy Dependence of Product Channel Branching Ratios. When a molecule is excited to an energy level above the threshold energies for two different product channels, it can, in principle, dissociate in two different ways. The higher the photon energy, the more dissociation channels are open. For example, depending on the available energy, an excited diatomic molecule can dissociate into an extended series of product channels, characterized by the states n, m of the atomic products:

$$\mathrm{AB} + \hbar\omega \rightarrow \mathrm{A}(n) + \mathrm{B}(m) \qquad (2)$$

Dissociation of polyatomic molecules can give rise to chemically different channels whose branching ratios are often strongly energy dependent. Typically, at the lowest energy, the mechanism of dissociation is a simple bond cleavage, a two-center process. As the photon energy increases, dissociation takes place by three and four center mechanisms and atomic migration takes place over an internal barrier producing molecular fragments. For example, CH_2O near its threshold dissociates into the radical pair H and HCO with an increasing formation of the molecular pair, H_2 and CO, as the photon energy increases.[26] This branching ratio is an important factor in determining the concentration of HO_2 radicals in the Earth's troposphere by the reaction $\mathrm{CHO} + \mathrm{O_2} \rightarrow \mathrm{HO_2} + \mathrm{CO}$. An extensive study has been carried out on the energy dependence of the photodissociation channels of HNCO.[27] As the photon energy was increased the lowest energy product channel CO + $\mathrm{NH}(\mathrm{X}^3\Pi)$ was gradually replaced by H + NCO and the latter was, in turn, replaced by CO and $\mathrm{NH}(\mathrm{A}^1\Delta)$. In fact, when exciting in the VUV, H + $\mathrm{NCO}(\mathrm{A}^2\Pi)$ are observed.[14] A particularly detailed study has been made on the photon energy dependence of the photodissociation of ethylene and its partially deuterated isotopomers.[28–30] After the photoprepared electronically excited ethylene crosses over to a vibrationally hot ground state molecule, the ground state dissociates at comparable rates into several channels. Vinyl radicals and hydrogen atoms are formed by a two-center bond rupture. Hydrogen molecules and both vinylidene and acetylene are produced by three- and four-center reactions, respectively. These branching ratios depend strongly on photon energy.

1.2. Velocity Distribution of Photofragments. Prior to around 1970 it was understood that when a molecule dissociated into two fragments, their momenta were equal and opposite and that the maximum relative translational energy was the difference between the photon energy and the energy required for dissociation. Aside from these verities the molecular gas was an impenetrable system. The modern age of photodissociation began with experiments intended to measure the velocity distribution of photofragments. The underlying philosophy was the same as that used in crossed molecular beam reactions. The collision or in this case the dissociation was to be regarded as a problem in classical or quantum mechanics, in which a point representing the system moved on excited and ground state surfaces toward its asymptotic destination. The equations of motion could be solved and the results compared with experiment.

When a molecule AB is dissociated into two fragments, A and B, the available energy, E_{avl} is defined by the conservation of energy equation:

$$E_{\mathrm{int}}(\mathrm{AB}) + \hbar\omega = D_{\mathrm{o}}(\mathrm{A{-}B}) + E_{\mathrm{avl}},$$
$$E_{\mathrm{avl}} = E_{\mathrm{t}} + E_{\mathrm{int}}(\mathrm{A}) + E_{\mathrm{int}}(\mathrm{B}), \qquad (3)$$

or, in other words, the internal energy of the parent molecule plus the photon energy is equal to the dissociation energy plus the relative translational energy plus the internal energy of the fragments. If the thermal motion of the parent molecule AB is neglected, the total kinetic energy release E_{t} is subdivided among the fragments in a fixed ratio, $m_{\mathrm{A}}/(m_{\mathrm{A}} + m_{\mathrm{B}})$ or $m_{\mathrm{B}}/(m_{\mathrm{A}} + m_{\mathrm{B}})$. The relative translational energy can be written as

$$E_t = [m_A m_B/(m_A + m_B)]v^2/2 \quad (4)$$

where $v = |\boldsymbol{v}_A - \boldsymbol{v}_B|$ is the relative speed between the fragments. Speeds of fragments can be determined by time of flight methods,[22,24,25] by the Doppler broadening of absorption lines of light fragments, or by velocity map imaging.[31–33] For diatomic molecules, a fixed photon energy and fixed final states of the atoms yield a fixed translational energy. In the case of a polyatomic molecule where there are many other ways of distributing the excess energy besides translation, the distribution of the latter is often very broad. A generalization can be made on the release of kinetic energy. A large kinetic energy would result from a descent on a strongly repulsive surface. The wave function would rapidly become highly oscillatory and the associated transition dipole matrix elements would become very small. In other words, rapid oscillation of the wave function greatly diminishes the overlap integral of the ground and excited state wave functions. An open channel with less kinetic energy would have larger transition matrix elements with the ground state. Thus, in general, nature prefers lower kinetic energies.

Linearly polarized light whose electric field has a specific direction in space can generate an anisotropic distribution of velocities of photofragments originating from molecules oriented randomly in the gas phase. This anisotropy is made possible by the fact that, in general, molecules are anisotropic absorbers of light. The principal interaction of light with molecules is through the electric field of the light wave and the electric dipole moment of the molecule. The latter is a vector, each of whose matrix elements has a specific direction in the framework of the molecule; therefore the absorption coefficient will be anisotropic. The maximum probability for absorption occurs when the transition dipole moment happens to be parallel to the electric vector of the light as shown in Fig. 2. Thus polarized light creates a set of excited molecules whose axes are anisotropically distributed. For instance, for a parallel transition in a diatom, the transition moment lies parallel to the internuclear axis. Hence, the parallel transition leads to a preferential excitation of molecules that are oriented parallel to the electric vector. If the recoil time of the fragments is short compared to the parent molecule's rotation time, i.e., direct dissociation, the fragments will appear in a $\cos^2\theta$ distribution, thus preferentially parallel to the laser polarization. Likewise, a perpendicular transition would yield a $\sin^2\theta$ distribution. These two photofragment angular distributions are the two extremes for a dissociation process following a one-photon excitation through an electric dipole transition:

$$I(\theta) = \frac{1}{4\pi}[1 + \beta P_2(\cos\theta)] \quad (5)$$

where β is the anisotropy parameter, θ is the angle between the electric vector and the recoil velocity vector, and $P_2(\cos\theta)$ is the second order Legendre polynomial. Equation 5 is the first of a number of correlation relations in photodissociation.[34–37] The direction at which fragments are ejected is correlated with the direction of the electric field of the photon. Equation 5 shows that the angular distribution is characterized by one parameter, β, which ranges from -1 for a perpendicular transition to $+2$ for a parallel transition. If $\beta = 0$ the distribution is isotropic in space.

Generally, the anisotropy parameter is given by,

$$\beta = 2P_2(\cos\chi) \quad (6)$$

where χ is the angle between the transition moment μ and the recoil velocity vector, $\boldsymbol{v}$. Thus, β is a function of molecular structure. The values of β determined by Equation 6 can only be obtained if the dissociation lifetime τ of the excited state is much shorter than the rotation period τ_{rot} of the parent molecule. If this condition is not fulfilled, the anisotropy of the angular distribution is lowered according to

$$\beta(\tau) = 2P_2(\cos\chi)\cdot\frac{\omega^2\tau^2+1}{4\omega^2\tau^2+1} \quad (7)$$

where ω is the molecule's angular velocity. For the very slow dissociation processes ($\tau >> \tau_{rot}$) the anisotropy is therefore lowered by a factor of 4. Lowering of measured anisotropy parameters is also seen if two different transitions with different signs in β (parallel and perpendicular transitions) occur simultaneously.

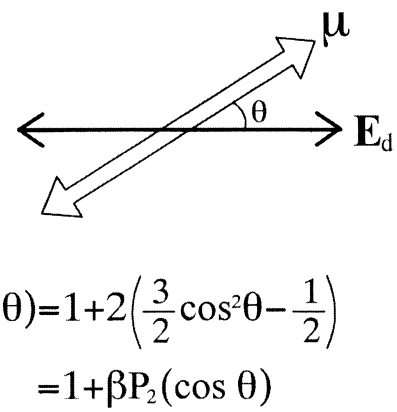

Fig. 2. Transition dipole moment $\boldsymbol{\mu}$ and electric vector $\boldsymbol{E}_d$ of dissociation light. See Eq. 5 for the angular distribution of the photofragment.

1.3. Internal State Distributions of Photofragments. The dynamics of photodissociation can be studied by measuring the angular distribution of the photofragments, their kinetic energy distribution and the time required for their formation. However, the internal state distribution of the fragments is the method that has been used most commonly and it is extremely informative. These distributions can be determined conveniently if the fragments can be excited to fluorescent states or to resonant intermediate states on the path to ionization. Almost any atom can be so probed. The important molecular fragments which have been probed include the diatomics, OH, CN, NH, CO, NO, H_2, N_2, MH(M = Li to Cs), CS, SO, HF and the polyatomics, NCO, HCO, SO_2, CO_2, CH_2, and CF_3. HF and CO_2 have been probed by infrared fluorescence. CH_3 and other polyatomic radicals have been probed by resonance-enhanced multiphoton ionization (REMPI) detection of fragments,[38,39] or by one-photon VUV ionization.[40] Laser probing of fragments is well suited for this purpose, because only those fragments that are in the probed state (electronic, vibrational, and rotational) will appear in the spectrum.

Rotational distributions are usually determined by measuring the relative intensities of the rotational lines of laser induced fluorescence excitation spectra. High-resolution velocity distributions from the time-of-flight and velocity imaging spectra can also reveal the rotational distributions by energy conservation in Equation 3.[41–43] This elegant method has been made even more elegant by the ability to lower the rotational temperature of the precursor molecule to a few K by expansion through a nozzle.[44] Angular momentum is generated by torques. If a linear triatomic molecule preserves its bond angle in the upper state before dissociating, the fragments will be rotationally cold. For example, when the linear molecule OCS is excited at 157 nm to a linear upper state, the CO molecules are rotationally cold.[45] The same is true of the OH radicals formed in the A ← X transition in H_2O, in which the separating H atom retreats along the original O–H bond direction.[46] Because an H atom is much lighter than an O atom, the center of mass in an OH group lies almost at the center of the O atom. Thus, the torque induced by the leaving H photofragment atom is small and causes no rotational excitation in the OH group. The opposite is true for the B ← X transition in water following which the bent HOH bond opens to nearly a linear structure before dissociation occurs, inducing a large torque.[47] The OH radicals so produced are rotationally hot.[8] The XCN triatomics (X = H, Cl, Br and I) all have linear ground states and bent upper states. The resulting torque produces rotationally hot CN radicals.[48]

1.4. Adiabatic and Nonadiabatic Photodissociation. Photolysis of a diatomic molecule can be understood in terms of two contributing processes as shown in Fig. 3: (i) the initial absorption of radiation populates one or more electronically-excited potential energy surfaces (PESs) at the molecular region, and (ii) subsequent fragmentation proceeds either adiabatically on the originally excited PES or through nonadiabatic transitions between surfaces at the asymptotic region. The contribution of each of these steps in describing the photodissociation dynamics and product branching depends sensitively on the forms of the PESs. Non-adiabatic transitions occurring at the asymptotic region can affect the relative yield of different product channels at the atomic region. In other words, branching ratios among the fine structure levels of open-shell atoms produced in photodissociation are determined not only by correlations between molecular and atomic states but also by adiabaticity of the dissociation process. In the UV photoabsorption of Cl_2, the $^1\Pi_u(1u)$ state of Cl_2 correlates to two $Cl(^2P_{3/2})$ atoms, while the $^3\Pi_u(0_u^+)$ state of Cl_2 correlates to the combination of $Cl^*(^2P_{1/2})$ and $Cl(^2P_{3/2})$. The $Cl^*(^2P_{1/2})$ state lies 2.5 kcal mol^{-1} above the $Cl(^2P_{3/2})$ state. In the wavelength range between 375 and 475 nm, the translational energy of the Cl photofragments from the photodissociation of Cl_2 is low and the dissociation processes from the photoexcited Cl_2 states are entirely adiabatic, that is, the Cl atoms from the $^1\Pi_u(1u)$ state of Cl_2 has an angular distribution with $\beta = -1$, while the Cl^* atom distribution from the $^3\Pi_u^+(0_u^+)$ state has $\beta = 2$.

$$\begin{aligned} Cl_2(X^1\Sigma_g(0_g^+)) + \hbar\omega &\rightarrow Cl_2(^1\Pi_u(1_u)) \\ &\rightarrow Cl(^2P_{3/2}) + Cl(^2P_{3/2}), \\ Cl_2(X^1\Sigma_g(0_g^+)) + \hbar\omega &\rightarrow Cl_2(^3\Pi_u(0_u^+)) \\ &\rightarrow Cl(^2P_{3/2}) + Cl^*(^2P_{1/2}). \end{aligned}$$

The ratios of absorption coefficients for the $^1\Pi_u(1_u) \leftarrow X^1\Sigma_g(0_g^+)$ and $^3\Pi_u^+(0_u^+) \leftarrow X^1\Sigma_g(0_g^+)$ transitions in this wavelength range can be derived from the obtained branching ratios. However, at 308 nm, and hence, when the translational energy of the Cl photofragments is increased, the dissociation becomes nonadiabatic. At 308 nm, Cl^* appeared with $\beta = -0.7$, which was nonadiabatically produced from the $^1\Pi(1_u)$ state.[49]

The following is an interpretation of the adiabatic and nonadiabatic processes in electronically excited Cl_2.[49] The five 1u electronic states of the $C1_2$ molecule arise from two ^2P_J (J = 1/2 or 3/2) chlorine atoms. In the adiabatic approximation, the lowest two l_u states (including the $^1\Pi(1_u)$ state) correlate to Cl + Cl, while the next two l_u states correlate to Cl + Cl^* and the final 1_u state correlates to $C1^*$ + $C1^*$. In the asymptotic region, as schematically shown in potential curves for a diatomic molecule (Fig. 3), these adiabatic PESs asymptotically become degenerate with the free atom energies that are split by units of 2.5 kcal mol^{-1}. When the speed of the separating atoms is high enough, nonadiabatic couplings among the lu states can take place according to the selection rule for the mixing with the nuclear kinetic energy operator ($\Delta\Omega = 0$). The degree of adiabaticity is expressed by the following relation, which corresponds to the ratio of the dissociation lifetime to the electron precession time due to the spin-orbit interactions:

$$\xi = (\Delta R/v)/(\hbar/\Delta E) \tag{8}$$

where ΔR is the length of the asymptotic interaction region, v

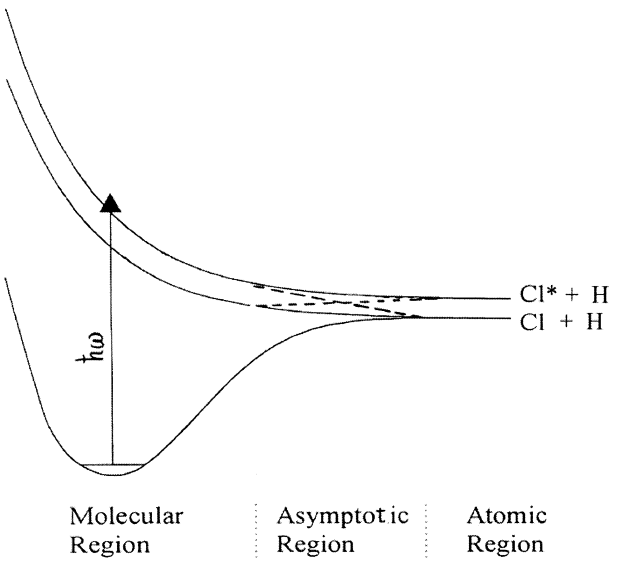

Fig. 3. Schematic of interaction between two potential energy curves: The solid curves represent adiabatic potential curves, and the broken ones show non-adiabatic potential curves for production of $Cl(^2P_{3/2})$ + H and $Cl^*(^2P_{1/2})$ + H from HCl. An electronic transition by photoirradiation occurs in the molecular region. Non-adiabatic interaction among potential energy curves occurs in the asymptotic region.

is the relative speed of the separating atoms, and ΔE is the energy separation of the interacting states. For $\xi << 1$ the system is in the sudden regime and the dissociation takes place diabatically, while for $\xi >> 1$ the dissociation proceeds adiabatically. For a fast separation speed of the photofragments with a large kinetic energy, the adiabaticity parameter ξ is small because there is no time for the electron to presses. In this case, both $J = 3/2$ and 1/2 are generated as the final photoproducts. In the diabatic limit, the ratios of [Cl*]/[Cl] are calculated to be 1/2 for the $^1\Pi_u(1u)$ state and 1 for the $^3\Pi_u{}^+(0_u{}^+)$ state using transformation coefficients between the molecular and atomic states.[50] The above discussion clarifies the contribution of the nonadiabatic dissociation from the $^1\Pi_u(1u)$ state at 308 nm.

Theoretical studies have established that the first UV absorption band of HCl arises predominantly from transitions from the ground X state to the repulsive $A^1\Pi$ state. A small ($< 0.5\%$) contribution to the total oscillator strength is predicted to occur only at long wavelengths from excitation to the repulsive $a^3\Pi$ state. At 235–190 nm, HCl can dissociate via two thermodynamically accessible product channels via the following adiabatic processes as schematically shown in Fig. 3:[51–60]

$$\mathrm{HCl} + \hbar\omega \rightarrow \mathrm{HCl}(\mathrm{A}^1\Pi) \rightarrow \mathrm{H} + \mathrm{Cl}(^2\mathrm{P}_{3/2}),$$
$$\mathrm{HCl} + \hbar\omega \rightarrow \mathrm{HCl}(\mathrm{a}^3\Pi_0{}^+) \rightarrow \mathrm{H} + \mathrm{Cl}^*(^2\mathrm{P}_{1/2}).$$

Since the measured β value of the H fragment at 193 nm was close to -1, the 193 nm transition is mostly perpendicular. However, non-adiabatic transitions occur as the molecule breaks apart. The Cl* channel constitutes a significant fraction of the total product yield: [Cl*]/[Cl] = 2/3 at 193 nm and 1/2 at 235 nm. The initial population associated with the state is redistributed at relatively large $A^1\Pi$ internuclear separation between all the $\Omega = 1$ states correlating to the Cl and Cl* channels, that is, the $A^1\Pi$, $a^3\Pi_1$, and $t^3\Sigma_1$ states.

1.5. Time Dependence of Dissociation. "There is nothing new under the sun."[61] The time dependence of photodissociation has been studied for three quarters of a century, first implicitly and later explicitly. The earliest observations were that in some spectra the rotational lines were unusually broad and became ever broader the greater the photon energy. By the uncertainty principle this breadth was inversely related to the lifetime, which, for example, must be of the order of picoseconds for BrO, SH, and HNO in the first electronically excited state.[62] Another example is the predissociative broadening by the crossing of dissociative states. The phenomenon of predissociation has also been observed with the gradual decrease of fluorescence lifetimes as a function of the rotational levels in $SD(A^2\Sigma)$.[63]

Observation of the angular distribution of fragments allows an alternate *implicit* measure of lifetime according to Eq. 7. The measurements in the time domain of single bond dissociations are *explicit*. At the fastest time scales these measurements are the Fourier transforms of what was long ago measured in the frequency domain. To begin with, dissociations take place either directly on an excited state potential surface, or indirectly on the ground state surface. If dissociation is on an excited surface whether it is the initially excited state or one close to it, dissociation is fast. For example, if a fragment achieves a terminal speed of 10^5 cm/s and reaches a terminal energy after traveling about two angstroms, the dissociation time is very roughly 100 fs, much faster than a typical rotation period. Hydrogen atoms, being light, when dissociating from excited states have an order of magnitude larger terminal velocities and an order of magnitude shorter times of separation.

In Zewail's famous experiment a fs pulse was applied to ICN and a subsequent fs pulse was used to probe the CN fragment by laser-induced fluorescence.[64]

$$\mathrm{ICN} + \hbar\omega \rightarrow \mathrm{I}\cdots\mathrm{CN} \rightarrow \mathrm{I} + \mathrm{CN}$$

There was a delay before the CN fluorescence could be observed after which the laser-induced fluorescence intensity increased to a constant maximum. The interpretation of this rise time was that it was the time required for the I–C bond to break. Just when a bond can be said to have broken is hard to define. More precisely it was the time required for the CN radical to be sufficiently far from the I atom that it exhibited the same absorption as that of the bare radical.[65] This rise time was about 100 fs.

In the time before a collision occurs, if the excited molecule crosses to the ground state, energy is conserved and the ground state is a strongly vibrationally excited "hot" ground state. A general statistical theory, RRKM (Rampsberger, Rice, Kassel and Marcus) enables the calculation of the rate of dissociation. The necessary assumptions are that the vibrational energy is statistically distributed among the molecular vibrational modes and that there is a transition state, a surface of no return whose structure and vibrational frequencies are known or calculable.

In the most common case a molecule's lowest optically accessible excited state lies considerably above the minimum energy required for dissociation. An extreme example is the hydrogen molecule whose bond energy is 4.4 eV but whose first electronic absorption is at 9.0 eV. A typical case is that of $(CH_3)_3N$, whose UV absorption produces fluorescence and predissociation via the hot ground state. As the photon energy increases, the internal conversion rate increases shortening the fluorescent lifetime, and its dissociation rate is calculated by the RRKM theory.[66]

$$\begin{aligned}(\mathrm{CH_3})_3\mathrm{N} + \hbar\omega(\lambda > 250\ \mathrm{nm}) &\rightarrow (\mathrm{CH_3})_3\mathrm{N}^* \\ &\rightarrow (\mathrm{CH_3})_3\mathrm{N} + 300\ \mathrm{nm},\\ (\mathrm{CH_3})_3\mathrm{N} + \hbar\omega(\lambda < 250\ \mathrm{nm}) &\rightarrow (\mathrm{CH_3})_3\mathrm{N}^* \rightarrow (\mathrm{CH_3})_3\mathrm{N}^{\neq} \\ &\rightarrow \mathrm{CH_3} + (\mathrm{CH_3})_2\mathrm{N},\end{aligned}$$

where * stands for the electronically excited state and $\neq$ for the vibrationally excited ground state. Another typical case is that of toluene. At a high enough energy the hot molecule slowly dissociates, primarily into a benzyl radical and a hydrogen atom. With 193 nm excitation the lifetime is 300 ns, a proof of an indirect dissociation.[67] Ketene, CH_2CO is an exceptional case in that it absorbs light, albeit weakly, at the threshold for forming $CH_2(^3B_1) + CO(X^1\Sigma)$. Delicate high resolution experiments have provided a more stringent test of the RRKM theory showing that there are discontinuities in the rate of dissociation as the photon energy is increased above the threshold energy.[68] The discontinuities arise from discontinuities in the numbers of available quantum states. The photofragments of

an even larger molecule, 1-iodonaphthalene exhibit angular anisotropy proving that its lifetime estimated from Eq. 7 is a ps or less and therefore dissociation must be direct from an excited state on a time scale of no longer than a picosecond.[69]

1.6. Multiphoton Dissociation. 1.6.1. Coherent and Incoherent Emissions and Absorptions. At ordinary field strengths Maxwell's equations are linear in the electromagnetic fields. However, the electric and magnetic susceptibilities, properties of the media in which the fields exist do depend very slightly on the strength of the field. At the very high field strengths produced by a focused laser, the electromagnetic field equations become nonlinear. Some consequences were first analyzed theoretically by Goeppert-Mayer in 1931.[70] Invention of the laser enabled the experimental study of coherent absorption processes involving two or more photons. At the outset we must distinguish between coherent and incoherent multiphoton emission and absorption.[71] Consider first multiphoton emission. An atom or a molecule when excited to a high energy level decays by a cascade of photons, a series of incoherent emissions descending the ladder of energy levels. In a few special cases such as the 2s state of an H atom or He^+ ion, the atom can only decay radiatively by a two-photon emission which is necessarily coherent.[72] Similarly, a two-photon absorption in which the intermediate state is virtual is also coherent. On the other hand a succession of two or more independent absorptions from lower levels to higher levels is incoherent. This means that the different absorption matrix elements have random phases. A coherent absorption process involves simultaneous absorption of two or more photons. There is a single overall matrix element for the entire process consisting of a product of matrix elements with definite phase relations. Coherent multiphoton processes can be tested by changing the polarization of the incident laser light from linear to circular. The absorption coefficient decreases if the transition is parallel or is between two electronic states with the same symmetry. It increases if the transition is perpendicular or is between states with different symmetries. A typical case is that of the two-photon absorption of Br_2 with linearly and circularly polarized light. The Q-branch absorption for the $\Delta\Omega = 0$ transition is diminished by two circularly polarized photons, while those of S- and O-branches are enhanced, comparing to those with two linearly polarized photons.[73]

An interesting test is a measurement of the angular anisotropy β of photofragments in two-photon dissociation with a ns laser. Multiphoton processes via real state(s) are often used for study of multiphoton dissociation dynamics. If the first photon excites the ground state molecule to a repulsive state ($\tau = 0$ in Eq. 7), the photon-molecule interaction time in the second photoexcitation step is short. After the second ns photon promotes the molecule in this repulsive state to a higher repulsive state, then, photofragments are produced. The angular distribution of the photofragment from the higher repulsive state reflects both the first and second angular distributions:

$$I(\theta) = [1 + \beta_2 P_2(\cos\theta) + \beta_4 P_4(\cos\theta)]/4\pi \quad (9)$$

where $P_4(\theta)$ is the fourth order Legendre polynomials. The intermediate repulsive state becomes practically virtual. On the other hand, if the intermediate state is bound and its lifetime τ is considered to be infinite in Eq. 7, memory of the molecular phase created by the interaction of the first photon with the molecule in the bound state is lost before the molecule absorbs the second ns photon. In this case, the angular distribution is well represented by Eq. 5 and not by Eq. 9, reflecting only the second photodissociation dynamics (as if it were a one-photon process as for the angular distribution). Experimental results for these two cases are clearly derived for NO_2, CS_2, and CH_3ONO.[74] The photodissociation of CS_2 at 300 nm first generates the bound CS_2^* state (this state can fluoresce), and then this bound state absorbs another 300 nm photon to decompose into S + CS. Angular distribution of the S atom is well represented by Eq. 5 because the intermediate CS_2^* has a long lifetime on the time scale of a ns laser pulse. Irradiation of NO_2 at < 398 nm produces the repulsive NO_2 state that absorbs another photon to decompose into O + NO. In this case, the angular distribution of the NO fragment is represented by Eq. 9 because the intermediate NO_2 has a quite short lifetime. If a fs photon is utilized, this kind of difference will not appear because the photon-molecule interaction is essentially coherent.

1.6.2. Vibrational Excitation Followed by Electronic Excitation. The ultimate key to understanding a direct dissociation is knowledge of the excited state potential energy surface(s) on which the dissociation occurs. One way of studying these surfaces is to observe the change in quantum state distributions and relative yields of the various product channels by altering the photon energy. Such a study is made more effective if the absorption spectrum itself contains information on the excited state. A nice example is HONO whose spectrum in the 390 to 300 nm range has vibrational structure corresponding to the N–O stretch in the upper state.[75]

A more profound method of probing involves Crim's "vibrationally mediated photodissociation". The molecule is excited vibrationally, in practice by an overtone of the O–H or N–H stretch, and then photodissociated by a UV photon. The yields and state distributions can be compared with those obtained by photodissociation using a single UV photon with the same energy as the total energy of the other two. When the HOD molecule is excited with four quanta in the O–H stretch, the ratio of the decomposition channel OD + H to that of OH + D is > 15 because the coupling between the two vibrational modes is weak.[76] At a still higher energy, selectivity is lost and the same ratio becomes unity. When HNCO is excited with a single photon of energy 44440 cm^{-1}, the yield of $NH(a^1\Delta)$ + CO is about 0.8 and that of H + NCO is about 0.2.[77] However when the N–H bond is excited with three quanta and the molecule is dissociated using the same total energy, the product yields are reversed. The yield of H + NCO is now 0.8 and that of $NH(a^1\Delta)$ is 0.2. The wave packets projected onto the upper surface from the vibrationally excited molecule and from the ground state molecule are largely located in different regions of the potential surface leading to very different outcomes. In general, the vibrationally hot ground state molecule has an enhanced photodissociation quantum yield. This effect will be discussed below in detail in connection with the dissociation of ozone.

1.6.3. Infrared Multiphoton Dissociation. The outstanding example of incoherent multiphoton absorption applied to photodissociation is the use of a CO_2 laser. For example, when

a typical CO_2 laser with photon energies near 1000 cm^{-1} is focused in SF_6 gas, photons are absorbed at a rate of the order of one/nanosecond.[78] After about 40 photons are absorbed an F atom and an SF_5 radical are produced. The time interval between absorptions is much longer than the dephasing time caused by internal vibrational redistribution, particularly at high energies. This multiphoton absorption has been likened to driving a system up a ladder of equally spaced energy steps. The metaphor fails both because of anharmonicity and the fact that the density of states becomes large after the absorption of several photons. This large density of states means that at energy of a few thousand cm^{-1} the molecule becomes "black", i.e. it absorbs all wavelengths. Only those molecules whose vibrational absorption overlaps the infrared laser output are observed to dissociate. Thus the initial few absorption steps are resonant. After that, many more photons are absorbed by the "black" molecule until dissociation occurs. The question of how much above threshold absorption occurs has bedeviled this type of experiment. The relative rates of dissociation and absorption are not well enough known. This ratio must surely depend upon the laser power. With this IR multiphoton technique reactive atoms and radicals are easily produced in a reaction gas cell filled with a reactant. The reactions of F atoms are easily tested with the infrared multiphoton production of SF_6.[79]

2. Control of Photodissociation Dynamics

2.1. Coherent Control of Phototransition. The coherent absorption of n photons each of energy $\hbar\omega$ does not necessarily produce the same result as the absorption of a single photon of energy $n\hbar\omega$. The reason is that each photon has a matrix element with a separate Franck–Condon factor. The product of n such factors will usually leave the system with a different spatial distribution on the dissociating state surface than the direct absorption of a single energetic photon. However, if the final products are the same, the n-photon absorption is merely a possibly more convenient way to reach the dissociative surface. Coherent multiphoton transitions make possible a subtler means of control of the branching ratios of product channels than simple energy variation.

One method of control, originally proposed by Tannor and Rice envisioned an excitation (PUMP) of a molecule to an excited surface by a very short light pulse.[80] The wave packet thus generated would move to a different region of the excited surface and then a second very short light pulse would cause a deexcitation (DUMP) to a lower surface on which selective dissociation would occur. Prudent selection of the shapes and relative timing of the two pulses would enable control of the product branching ratios. The PUMP-DUMP scheme has been successful but in an application strikingly different from those originally proposed. Averbukh et al. excited Br_2 molecules with a fs visible light pulse.[81] The roughly 100 fs pulse was sufficiently short that it excited a wave packet of vibrational states on the upper B state. This wave packet initially diffuses but because it has a finite number of components eventually returns to its initial relatively narrow shape. At that time a second light pulse nonresonantly ionizes the molecule. The recurrence or revival time is different for different isotopes. Thus at the instant when a ^{79}Br–^{79}Br molecule wave packet has revived, a ^{81}Br–^{81}Br molecular wave packet may still be quite diffuse and therefore only weakly absorbing. In this way isotope separation has been achieved.

The other method of the popular inversion is controlled by fs chirp pulses or the photon frequency is temporally changed in a time scale of ps. Chirp is naturally caused by the propagation of laser pulses through matter, which leads to group velocity variations as a function of frequency within the pulse, thus causing a frequency sweep. A positive chirp is a pulse in which the leading edge of the pulse is red shifted and the trailing edge is blue shifted with respect to the central frequency of the pulse. A negative chirp corresponds to the opposite effect. Wilson and co-workers investigated chirp effects on three-photon absorption yields in I_2 vapor using tailored fs pulses.[82a] Tailored pulses can be used to enhance single and multiphoton excitation with a factor of 3. After CH_2I_2 absorbs five visible fs pulses, it is excited effectively to the VUV energy region,[82b] and then it produces electronically excited I_2 that emits UV light as stated in the first section.[12]

$$CH_2I_2 + 5\hbar\omega(624\ \text{nm}) \rightarrow CH_2 + I_2(D'^3\Pi_{2g}),$$
$$I_2(D'^3\Pi_{2g}) \rightarrow I_2(A'^3\Pi_{2u}) + 342\ \text{nm}.$$

This emission intensity changes as a function of the degree of negative and positive chirping. Temporal matching of the photon energy with the time evolution of the electronically excited state causes this change. Zhang et al. observed a factor of 2.9 in the overall change in the yield for this pathway as a function of chirp.[82b]

A second, rather different method of coherent control has been proposed by Shapiro and Brumer.[83] This method differs from that of the PUMP-DUMP scheme that uses tailored ultra fast pulses. Suppose that an optical excitation excites a molecule from its initial state to a specific state of dissociation products. Figure 4 shows a schematic of this type of experiment. When electronic excitation is accomplished by two different pathways, the probability of the process is obtained by adding the amplitudes for the different pathways and then squaring. Thus the probability will become dependent on the phase difference of the transition matrix elements between the two amplitudes. The following equations show the combined electric field $\boldsymbol{E}(t)$ and the excitation probability $P(\Delta\phi)$:

$$\boldsymbol{E}(t) = \boldsymbol{E}_1\cos(\omega_1 t + \phi_1) + \boldsymbol{E}_3\cos(\omega_3 t + \phi_3), \quad (10)$$

$$P(\Delta\phi) = {I_1}^3 A_1 + I_3 A_3 + 2(I_1 I_3 A_1 A_3)^{1/2}\cos(\Delta\phi), \quad (11)$$

A_1 and A_3 are proportional to the squares of matrix elements between the initial molecular state and the final state of the fragments. $I_1 = |\boldsymbol{E}_1|^2$ and $I_3 = |\boldsymbol{E}_3|^2$. The appropriate weak light fields are applied on a ns time scale and the degree of phase control is, so to speak, decided by the system and not by the experimenter. This is altered by varying the pressure of Ar or H_2 gas through which the two light beams travel before reaching the interaction cell for molecule and photons. The yield of each channel will vary sinusoidally with the relative phase $\Delta\phi$ where

$$\Delta\phi = \phi_3 - 3\phi_1 + \delta_{13} \quad (12)$$

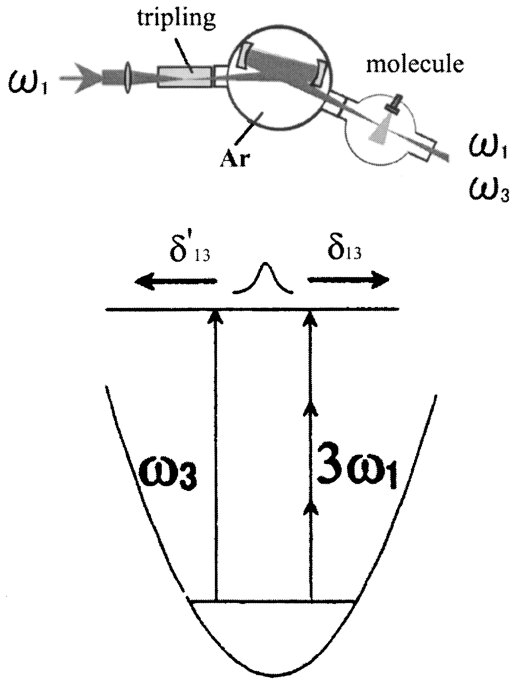

Fig. 4. Phase control of reaction branching. Modulation of the branching results from simultaneous irradiation of a molecule by a fundamental photon ω_1 and its third harmonic ω_3. The branching ratios depend on the phase difference between three fundamental photons and their third harmonic as defined by Equations 10–12. The phase difference of incoming laser photons is altered by varying the pressure of the gas (i.e. argon) through which the two light beams travel before reaching the detection chamber as shown by an experimental setup in the upper panel.

This scenario has been first applied to a number of areas of molecular spectroscopy, especially coherent control of UV photoabsorption. The interference phenomenon between applied waves of different frequency was first observed in Hg atom vapor by Elliott and coworkers.[84] Later Gordon and coworkers demonstrated interference between one and three photon amplitudes for excitation in relatively small molecules, HCl, CO, H_2S and CH_3I at 118 and 355 nm.[84] Bersohn and coworkers have demonstrated phase control of absorption in large polyatomic molecules in order to answer the question; "Can interference between one and three photon amplitudes be observed in molecules with much larger number of atoms than CH_3I in which many rotational states would be simultaneously excited?".[85] Interference was indeed observed in $N(CH_3)_3$, $N(C_2H_5)_3$, $(CH_3)_2N_2H_2$ and *c*-C_8H_8 at 201 nm and 603 nm. The 603 nm laser light was tripled in a gas cell and two laser beams were changed in relative phase in an Ar gas cell, as shown by the upper panel of Fig. 4.

$$(CH_3)_3N + [\hbar\omega_3(201\text{ nm}) + 3\hbar\omega_1(603\text{ nm})] \rightarrow (CH_3)_3N^* \text{ [controlled by } \Delta\phi]$$

They concluded that molecular size is no obstacle and that as long as a molecule has sufficiently strong absorption at the tripled frequency and has sufficient vapor pressure, phase control of interference is observable.

Most interesting applications to molecular photodissociation occur when two chemically different channels are open. If the phases of the transition matrix elements for the two different channels are not the same, that is, δ_{13} and δ_{13}' are different in Eq. 12, then, the yields of the two channels will be out of phase and therefore can be controlled by Eq. 11. An elegant example is the molecule HI that at a certain high energy can undergo either ionization or dissociation into a hydrogen atom and an iodine atom, probably in an excited state. By varying the relative phase as defined above, Gordon showed that the two channel phases are different and therefore the relative yields of the two channels could be varied sinusoidally.[84]

$$\begin{aligned} &HI + \hbar\omega_3 + 3\hbar\omega_1 \rightarrow HI^+, && \delta_{13} \\ &HI + \hbar\omega_3 + 3\hbar\omega_1 \rightarrow H + I. && \delta_{13}' \end{aligned}$$

Modulation of HI^+ and I^+ signals result from irradiation of HI with 353.80 nm light and its third harmonic. The HI^+ peak is the result of one or three photon ionization. The I^+ peak is derived from the product of a neutral dissociation into an H atom and an electronically excited I atom that is then REMPI ionized by absorption of an additional photon. The period of the oscillations depends on the phase difference between three fundamental photons and their third harmonic as shown by Eq. 11. Most importantly, note that the two chemically different exit channels of HI have different channel phases, or $\delta_{13} \neq \delta_{13}'$. The origin of the channel phase has recently been shown to depend on a coupling of the continuous dissociating state to a discrete state or to another continuum or to an intermediate state which is resonant with one optical process but not the other.[84] The channel phase vanishes if these conditions are not met, and hence, controllability by the photon phase is lost.

There will surely be more success in the future in the control of photodissociation pathways via the $(3\omega_1 + \omega_3)$ interference. However, the need for both strong three-photon absorption and frequency tripling will be limiting factors. Fortunately, there are other routes to phase control. In an experiment involving two colors, ω_1 and ω_2, the two-photon transition probability for absorbing both ω_1 and ω_2 is proportional to the square of the sum of two matrix elements.[84c] A very important observable for the photodissociation dynamics is the angular distribution of fragments. This angular distribution can be altered by varying the phase between one wave of frequency $\omega_2 = 2\omega_1$ and two waves of frequency ω_1. Two different final states are involved whose angular wave functions are orthogonal due to the transition selection rules, i.e., $g \leftrightarrow g / u \leftrightarrow u$ for the two-photon transition and or $u \leftrightarrow g$ for the one-photon transition. But those radial wave functions are not necessarily orthogonal. Thus if observations are made at a fixed angle, there can be interference if the total flux is averaged over all angles there would be no interference. To illustrate, suppose dissociation is very fast and the transition dipole axis and the axis of dissociation coincide. Then, the matrix element for one-photon absorption would be proportional to $\cos\theta$ and the angular distribution can be described by Eq. 5 with $\beta = 2$ and Fig. 2. Furthermore, the matrix element for two-photon absorption would be proportional to $\cos^2\theta$ if the virtual intermediate transition were parallel. The square of the sum of the two matrix elements would contain a term of odd parity, $\cos^3\theta$.

$$I(\theta) = [\cos(\theta + \Delta\phi) + \cos^2(\theta + \Delta\phi)]^2,$$
$$= \cos^2(\theta + \Delta\phi) + 2\cos^3(\theta + \Delta\phi) + \cos^4(\theta + \Delta\phi). \quad (13)$$

If the matrix elements were adjusted to be equal in magnitude, by phase control in $\Delta\phi$, most of the one photofragment, say, **A** fragment of **AB** molecule, would be sent in one direction and the other fragment, **B**, in the other. If we can set a proper trap for one particular fragment, we can effectively select the branching.

A third control method, "optimal control", proposed by Judson and Rabitz is completely empirical.[86] The light pulse is dispersed into many different frequencies each with its own amplitude and relative phase. These parameters are varied so as to improve constantly the yield of a given photoproduct. Gerber and Levis have obtained striking results with the use of a fs pulse combined with a liquid crystal spatial light modulator (SLM).[87] The very short pulse consists of many frequencies which are spatially dispersed by a grating into multiple frequencies, each with its own phase and amplitude. These are initially chosen randomly. The strong ($> 10^{13}$ W cm^{-2}) light pulse dissociates the molecule and ionizes the fragments although not perhaps in that order.[88] The signal due to a particular mass is fed back to the SLM where the various phases and amplitudes are adjusted until the yield of a particular ion is maximized or minimized. This extremely general method has been applied to the formation of CH_3CO^+ from CH_3COCH_3, both CH_3^+ and CF_3^+ from CH_3COCF_3, and both $C_6H_5CO^+$ and $C_6H_5^+$ from $C_6H_5COCH_3$.[87b] Most remarkable, a new product, toluene was formed from acetophenone; it is not observed with weak light fields.[87b] In other words, a strong light field has brought about a new dissociation channel. Much remains to be learned about the phenomena occurring in very strong laser fields.[88]

The original theoretical conception was that the PUMP and DUMP pulses would be tailored to fit the potential surface. To apply this method one would either have to have extensive knowledge of the potential surfaces or acquire this knowledge by repeated trials of different pairs of pulses. The successful feed back experiment is a *tour de force*, a triumph of engineering and empiricism. One learns nothing about the potential surface. One does not know how many of the 800 nm photons were used for pumping and how many for dumping. Nevertheless, effective control is exerted over competing channels of a photodissociation. Because the strong field does not have to be resonant, the method is not limited by spectroscopy and is very general.

2.2. Control of Dissociation Branching by Alignment of Parent Molecules. A neutral molecule placed in an electric field can be aligned because of the anisotropy of its polarizability tensor. As an alternative to high static electric fields, the electric field of a pulsed laser can be used for alignment. The control parameter γ of the degree of alignment for a linear or a quasi-linear molecule is:

$$\gamma = -(\langle\alpha\rangle - \alpha_{zz})(E^2/2kT)P_2(\cos\chi) \quad (14)$$

where $\langle\alpha\rangle$ is the mean polarizability, α_{zz} is the element of the polarizability tensor along the symmetry axis and E is the rms optical electric field. χ is the angle between the electric vectors of the aligning and dissociating lasers. If the electric vectors of the aligning IR and dissociating UV lasers are set parallel to each other, the observed anisotropy parameter, β_2, for $P_2(\cos\theta)$ in Eq. 5 is given by:

$$\beta_2 = \beta_o + \gamma(1 + 2\beta_o/7 - \beta_o^2/5) \quad (15)$$

where β_o is the anisotropy parameter in the absence of the aligning radiation. The angular distribution has been controlled in this way for I_2, CH_3I, CS_2, C_6H_5I, and OCS.[89–91] A recent experimental demonstration showed control of the branching ratio of two different photodissociation channels for I_2 and Cl_2 using aligned molecules.[92,93] The photodissociation of Cl_2 at 404 nm has two channels via adiabatic excited potential surfaces as described above. The molecules are either excited to the $B^3\Pi_u^+(0_u^+)$ state that dissociates into Cl + Cl*, or to the $^1\Pi_u(1_u)$ state that dissociates into 2Cl. The $B^3\Pi_u^+(0_u^+)$ state is connected to the ground $X^1\Sigma_g(0_g^+)$ with a parallel transition moment with $\beta_0 = 2$, whereas the transition moment from the ground state to the $^1\Pi_u(1_u)$ state is perpendicular with $\beta_0 = -1$. Selective excitation is obtained by controlling the spatial alignment of the molecules with respect to the polarization of the exciting light so that either parallel transitions are enhanced and simultaneously perpendicular excitations suppressed or vice versa. A strong nonresonant laser field controls the alignment of the molecules since the interaction between the induced dipole moment of the molecules and the strong linearly polarized laser field forces the molecules to align along the polarization axis according to Eq. 14.[93]

$$Cl_2 + 1.06\ \mu m \rightarrow Cl_2(\text{aligned})$$
$$Cl_2(\text{aligned}) + 404\ nm \rightarrow 2Cl(^2P_{3/2}) \text{ or } Cl(^2P_{3/2}) + Cl^*(^2P_{1/2}).$$

The upper panel of Fig. 5 shows that the anisotropy parameter ratio β_{eff}/β_2^0 of Cl increases with nonresonant IR laser intensity where β_{eff} and β_2^0 are the anisotropy parameters in the presence and absence respectively of the IR aligning laser. For each IR laser intensity the cross sections can be expressed in terms of the control parameter γ of Eq. 14 by the relations: $\sigma_{\parallel}^{\text{align}}$ is $1 + 2\gamma/5$ and $\sigma_{\perp}^{\text{align}}$ is $1-3\gamma/5$, where σ represents an absorption cross section. From the speed distributions of the Cl photofragments as shown by the inset of Fig. 5, we can determine the $\Phi_{\parallel}/\Phi_{\perp}$ branching ratio relative to the nonresonant laser field. The quantum yield $\Phi_{\parallel}$ of the Cl* + Cl channel increases while $\Phi_{\perp}$ of the Cl + Cl channel decreases with IR laser intensity, when the parent Cl_2 molecules are aligned along the IR laser polarization axis and the two channels correlate adiabatically with two excited potential energy surfaces accessed through a parallel and a perpendicular transition, respectively.

2.3. Control of Dissociation Branching by Upconversion via Bending Mode Excitation. OCS is linear in its ground state and bent in its first excited state. It serves as a model for the effect of bending on photodissociation dynamics. When OCS is excited in its first UV band, the following channel is the main dissociation pathway that produces rotationally hot but vibrationally cold CO molecules along with an S(^{1}D) atom,[91]

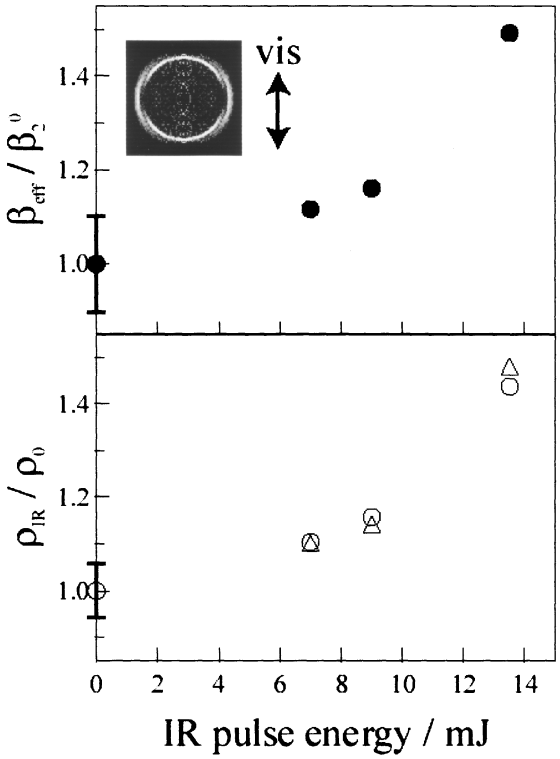

Fig. 5. The upper panel shows a change of the anisotropy parameter ratios β_{eff}/β_2^0 with 1064 nm laser intensity for $Cl(^2P_{3/2})$ photofragments from the photodissociation of Cl_2 at 404 nm (linearly polarized visible light, VIS). β_2^0 without IR laser. The VIS and IR lasers have parallel polarization. The inset shows a typical photofragment image (two circles) and the direction of the electric vector $\boldsymbol{E}$ of the dissociation VIS laser light (arrow). The outer circle corresponds to the Cl_2 + 404 nm → $2Cl(^2P_{3/2})$ process with the perpendicular transition while the inner circle to the $Cl^*(^2P_{1/2})$ + $Cl(^2P_{3/2})$ process with the parallel transition. The difference in the diameters of the two circles arises from the energy difference of 0.109 eV between Cl and Cl*. The lower panel shows changes of the $\Phi_\parallel/\Phi_\perp$ branching ratios with 1064 nm laser intensity. The open circle are the observed branching ratios with and without the 1064 nm IR laser pulse, $\rho_{IR}/\rho_0 = [\Phi_\parallel/\Phi_\perp]_{IR}/[\Phi_\parallel/\Phi_\perp]_0$. The open triangles are the ratios, ρ_{IR}/ρ_0, calculated from the anisotropy parameter ratios, β_{eff}/β_2^0.

$$OCS(v = 0) + \hbar\omega(UV) \rightarrow OCS^*(1^1\Delta(2^1A')) \rightarrow CO(X^1\Sigma^+, J) + S(^1D).$$

The potential curves are shown schematically in Fig. 6. Because bent states are involved in the UV dissociation, most of the available energy is allocated to the rotational motion of CO.

In the vacuum UV absorption band, S(1S) and CO are produced from the photodissociation via direct VUV excitation of the $^1\Sigma^+ \leftarrow X\ ^1\Sigma^+$ transition. At 154–157 nm the partition of internal and translational energy was investigated for this repulsive state.[45,95] Due to the linear structure of OCS and the stiffness of the C–O bond, a) most of the available energy is allocated to relative translational motion, and b) the angular

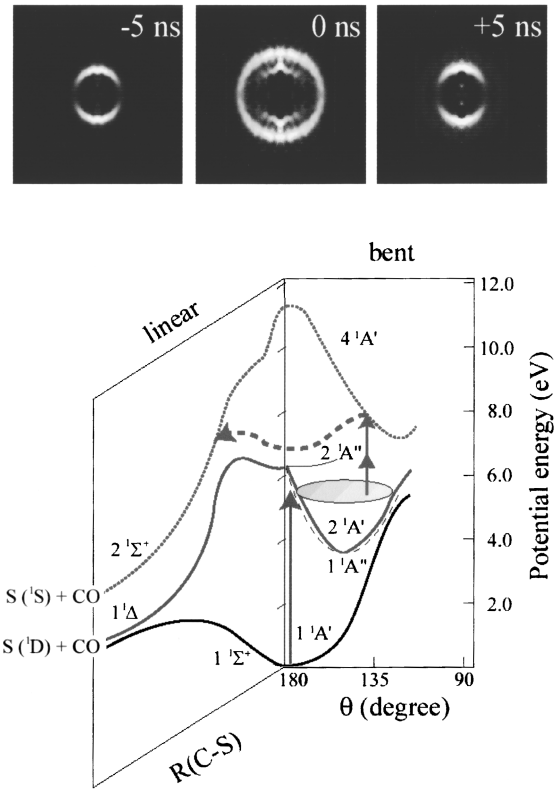

Fig. 6. Lower panel shows the potential energy curves of OCS as a function of bond angle θ and internuclear distance R. Up-going arrows from $OCS^*(2^1A')$ to $OCS^{**}(2^1A'')$ indicate the excitation processes for UV + 2IR photons. Left-going arrow indicates this dissociation pathway via bend and stretch modes Upper panel shows the images of CO from OCS. When the time delay between the UV and IR pulses is over 5 ns and hence the two laser pulses do not temporally overlap to each other, S(1D) atom is produced via $OCS^*(2^1A')$. When the two laser pulses temporally overlap to each other (delay = 0 ns), the up-conversion to $OCS^{**}(4^1A')$ from the strongly bent $OCS^*(2^1A')$ is completed and S(1S) is produced via $OCS^{**}(4^1A')$.

anisotropy is as high as $\beta = 1.8$. If a stepwise transition through the UV prepared OCS* occurs by multiphoton absorption to the VUV energy region, the dissociation pathway may be controlled. The upper repulsive state is prepared by infrared (IR) excitation at 1.06 μm through OCS*. Switching of the S(1D) formation to S(1S) is achieved by upconverting the lower electronic state with the IR photons. This method is different from Crim's vibrationally mediated photodissociation. The UV and IR laser pulses must overlap in time for the OCS* to absorb additional IR photons to produce S(1S). This situation is demonstrated by the images in the upper panel of Fig. 6.

$$OCS(v = 0) + \hbar\omega(UV) \rightarrow OCS^*(2^1A', \text{strongly bent}),$$
$$OCS^*(2^1A', \text{strongly bent}) + 2\hbar\omega(IR) \rightarrow OCS^{**}(4^1A'(2^1\Sigma^+)) \rightarrow CO(X^1\Sigma^+) + S(^1S).$$

After the additional two IR photons are absorbed, the excited OCS* crosses to the upper $OCS^{**}(4^1A'(2^1\Sigma^+))$ potential sur-

face that correlates with S(^{1}S) + CO. According to a quantum mechanical calculation, the vertical excitation energy of OCS** from the linear ground state is about 11 eV, far above the total energy of UV + 2IR (7.7 eV), as shown in the lower panel of Fig. 6.[94] However, the potential energy of OCS** is lowered in the bending coordinate, and the potential surface eventually intersects with OCS* in linear geometry at an extended bond length. Because the photoprepared OCS* has a deep minimum in the bending coordinate, it is excited to OCS** by two-IR photon absorption that results in formation of CO(J) + S(^{1}S) via crossing to OCS**. When the IR light intensity is so strong that the upconversion rate is much larger than the dissociation rate of the lower OCS* state, total upconversion of the lower repulsive state in the bent state is achieved.

3. Photochemistry of Hot-Molecules in the Earth's Atmosphere

Translational energy of a photofragment is calculated from its time-of-flight spectrum as shown in Fig. 1. In the case of diatomic molecules, the internal energy of the parent molecule appears in Eq. 3. The results for Cl_2 show that some of the Cl atom photofragments are faster than expected for dissociation of a cold molecule. The translational energy is calculated from Eq. 3 with vibrational energy of the hot parent molecule.[96] Formation of higher rotational levels of CO from OCS suggests the hot band channel even in an expanded molecular beam, which comes only from the bent OCS, 520 cm^{-1} above the ground level. At 289 K, 8% of the molecules are in $v_2 = 1$. There may be somewhat less in the expanded molecular beam but it is likely that a few % are still in the $v_2 = 1$ level because vibrational cooling in the molecular beam was not complete.[44] Thus, even if the fraction of the OCS($v_2 = 1$) level is small, the photoexcitation of the hot band is not negligible. This contribution is explicable in terms of the Franck–Condon factor for optical excitation from the $v_2 = 1$ level at the particular wavelength being much larger than that of excitation from the $v = 0$ level.

This is the case for the hot band dissociation of ozone under molecular beam conditions.[96,97] It is interesting to review the photochemistry of hot ozone under atmospheric conditions.[98] The quantum yields for production of the first electronically excited state of oxygen atom, O(^{1}D), in the ultraviolet photolysis of O_3 is a good example of the photochemistry of vibrationally excited molecules in the Earth's atmosphere. It is believed that vibrationally excited species do not play a major role in the chemistry of the Earth's lower atmosphere, since they are much less abundant compared to the ground state species under the atmospheric temperature condition. The most notable exception is the photodissociation of ozone below the thermodynamical threshold for the formation of O(^{1}D). The primary reason for the extreme importance of this very low abundance species is that O(^{1}D) reactions produce highly reactive species from unreactive species. Specifically, the OH radical in the stratosphere and troposphere are mostly produced from the reactions of O(^{1}D) with inert H_2O.

$$O(^1D) + H_2O \rightarrow 2OH$$

The major source of O(^{1}D) in the lower atmosphere is the photolysis of ozone in the Hartley and Huggins bands. Translationally hot O(^{1}D) is generated.[99] The strong increase in the ozone absorption cross section below 330 nm and the consequent absorption by overhead ozone leads to the sharp decrease of the solar actinic flux, which becomes practically zero below 290 nm in the lower stratosphere and troposphere. Because the photolysis of atmospheric ozone depends on the overlap of the wavelength dependent actinic flux and the ozone absorption cross section, the opposing wavelength dependence of these two quantities essentially restricts the photodissociation to 290–330 nm. This is precisely the wavelength region where O(^{1}D) production increases from near zero values around 330 nm to near unit values around 290 nm. Therefore, the calculated atmospheric O(^{1}D) production rate is very sensitive to changes in the quantum yield for its production in the photolysis of ozone in this wavelength range. It is also this region where the UV absorption cross sections of ozone and the quantum yields for O(^{1}D) production are highly sensitive to temperature because the formation pathway is due to a "hot" O_3 species. These changes in O(^{1}D) quantum yields are very important to atmospheric modeling. Talkudar et al. suggested that the contributions of the tail dissociation process due to the 290–330 nm tail can make the formation of O(^{1}D) five times larger at solar zenith-angle of 85° than the value estimated without them.[101] The importance of this O(^{1}D) channel is shown in the inset of Fig. 7 about the changes of the absolute yields of OH formation in the atmosphere, which shows the ratios of the OH concentration with and without the O(^{1}D) formation from the hot band dissociation process.

There are five energetically possible fragmentation pathways in the UV/vis photolysis of O_3:

$$O_3(v = 0) + \hbar\omega(\lambda < 310\ \text{nm}) \rightarrow O(^1D) + O_2(a^1\Delta_g), \quad \text{(I)}$$
$$O_3(v_3 = 1) + \hbar\omega(\lambda < 330\ \text{nm}) \rightarrow O(^1D) + O_2(a^1\Delta_g), \quad \text{(II)}$$
$$O_3(v = 0) + \hbar\omega(\lambda < 411\ \text{nm}) \rightarrow O(^1D) + O_2(X^3\Sigma_g^-), \quad \text{(III)}$$
$$O_3(v = 0) + \hbar\omega(\lambda < 1180\ \text{nm}) \rightarrow O(^3P) + O_2(X^3\Sigma_g^-), \quad \text{(IV)}$$

where the long wavelength limits given in parentheses indicate the thermodynamic thresholds for the fragmentations at 298 K when the parent $O_3(X^1A_1)$ molecule is excited from its v_3 vibrational level. For photodissociation in the Hartley band ($^1B_2 \leftarrow X^1A_1$) at $\lambda < 300$ nm, it has generally been accepted that channels (I) and (IV) are predominant, with the quantum yields of 0.9 and 0.1, respectively. In the UV Huggins band ($\lambda > 300$ nm), production of the O(^{1}D) atoms above 310 nm has been attributed to both channel (II) via the photodissociation of hot O_3, and (III) via the spin-forbidden dissociation. The contributions made by these excitation processes to the quantum yields for O(^{1}D) atom from O_3 photolysis are indicated in Fig. 7.

The structured part of the Huggins band at $\lambda = 310$–330 nm has been assigned as transitions to bound vibrational levels of a $^1A_1$ state reached in a two electron transition from the ground $^1A_1(0,0,1)$ state but with an odd quantum number change in the antisymmetric stretch mode v_3 (b_2 symmetry), making the overall symmetry $^1B_2$, and presumably gaining intensity from the nearby one photon $^1B_2$ state. Translational anisotropy measurements are consistent with a positive value of the translational anisotropy factor $\beta = 0.6$ that corresponds to transition

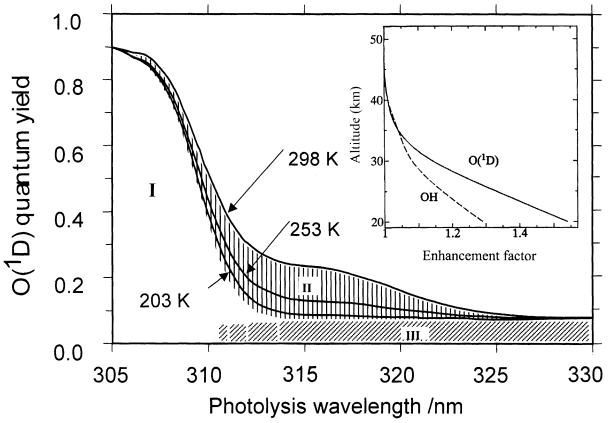

Fig. 7. $O(^1D)$ quantum yields from the O_3 photolysis for 203–298 K in the wavelength range 305–330 nm (Solid lines). Contributions made by the various dissociation processes to the quantum yields for $O(^1D)$ atoms are indicated in three different regions. Region I corresponds to excitation of the parent cold molecule and dissociation via channel, $O(^1D) + O_2(a^1\Delta_g)$. Region II (hatched area with vertical lines) indicates the contribution from the hot band excitation process leading to $O(^1D)$ formation via $O(^1D) + O_2(a^1\Delta_g)$, at 298 K, whose quantum yield is temperature dependent. Region III (hatched area with slash lines) represents the contribution from the spin-forbidden process via $O(^1D) + O_2(X^3\Sigma g^-)$, whose quantum yield is temperature independent. The inset shows a 1-box model calculation for the changes of the absolute yields of $O(^1D)$ atoms and OH radicals in the Earth's air. The enhancement factors of the $O(^1D)$ and OH concentration due to the hot band dissociation process of O_3 depend on the altitude because the UV spectral distribution around 300 nm from the Sun strongly depends on the altitude.

to the $^1B_2$ state. This process is temperature dependent. However, the temperature independent part of the $O(^1D)$ quantum yield in the Huggins band region above 320 nm is attributed to spin-forbidden process (III). The measured translational energy distributions of the $O(^1D)$ fragments are entirely consistent with those expected from process (III).

4. Photodissociation Processes as Reactive Radical Sources

The atom-diatomic molecular reactive scattering is one of the fundamental elementary chemical reactions[103] as well as one of the reaction processes in the Earth's air.[104] To study this process, an elaborate molecular beam scattering technique that requires massive construction has been used. Alternatively, a similar reaction system can be studied in a simple gas cell by probing the nascent product before it is relaxed by collisions in the cell.[68] For this type of experiment, photofragments with translational energies of a few eV are often used as reactants because the kinetic energy and angular distributions of the fragments are well characterized by Eqs. 3 and 5. The UV photodissociation of H_2S, HBr, HI, C_3O_2, NO, O_2, O_3, N_2O, SO_2, F_2, CS_2, HCl, Cl_2, Cl_2CO and Cl_2SO for example, produces H, C, N, O, F, S, and Cl, whose electronic states, energy and angular distributions are well defined as described above. Some examples are shown below.

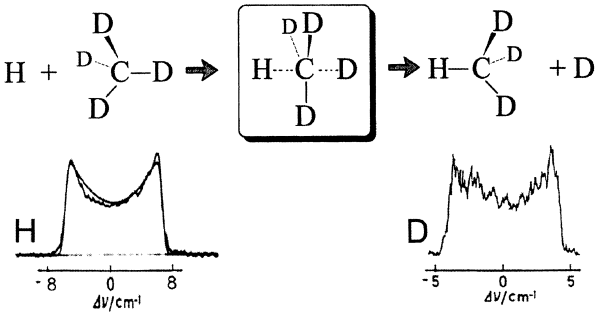

Fig. 8. Substitution reaction, S_H2 of a D atom in deuterated methane with a hot H atom. The H atom source is the photodissociation of H_2S with linearly polarized 193 nm. The Doppler profile of the H atom corresponds to $\beta(H) = -0.94$ with 2.5 eV translational energy. The solid curve is a fitted Doppler shape. The Doppler profile of the product D atom corresponds to $\beta(D) = -0.78$ and 80% of the original translational energy of the H atom, suggesting that the substitution reaction takes place almost collinearly.

When an H atom reacts with methane, both abstraction reaction and substitution reaction occur. Experimentally deuterated methane CD_4 was used in order to distinguish the product and reactant atoms. The source of the H atom was the photodissociation of H_2S with a linearly polarized 193 nm photon:[105]

$$H_2S + 193\ \text{nm} \rightarrow H + SH,$$
$$H + CD_4 \rightarrow HCD_3 + D.$$

The kinetic equation for the substitution reaction can be written:

$$d[D]/dt = k[H][CD_4] \quad (16)$$

where k is the rate coefficient and $[i]$ is the concentration of component i. If the probing laser is pulsed at a short time t later than the dissociating laser, the rate coefficient can be written

$$k = [D]/([CD_4][H]t) \quad (17)$$

k can also be written from kinetic theory as

$$k = <v\sigma(v)> \quad (18)$$

where $\sigma(v)$ is the cross section at relative speed v. Methane is so unreactive to H atoms that $\sigma(v = 2\ \text{km s}^{-1})$ is only 0.08 A^2. A proof that the reaction takes place by inversion is based on velocity anisotropies as shown in the lower panel of Fig. 8, in which Doppler shapes of the reactant H atom and product D atom are shown. The H atom is produced from the photodissociation of H_2S by a linearly polarized 193 nm photon. Since the 193 nm transition corresponds to $\beta(H) = -0.94$, the Doppler shape $g(\omega)$ of the H atom absorption has a dip in its center position:

$$g(\omega) = (1/v\omega_0)(1 - \beta/2)P_2[c\Delta\omega/\omega_0 v]\} \quad (19)$$

where ω_0 is the central frequency of the Lyman-α transition

and $\Delta\omega$ is its shift due to the fragment speed distribution. c and v are the speed of light and the speed of the fragment, respectively. The Doppler profile of the product D atom has an anisotropy similar to that of the reactant H atom. The dynamics of the substitution reaction are revealed by the energies (calculated from the Doppler width) and the anisotropy parameter ($\beta(D) = -0.78$ calculated from the Doppler shape) of the product D atom. The translational energies are 80% of the original translational energy of the H atom because the D atom rolls down the repulsive potential surface via the inversion reaction. One can show the average angle between product D and reactant H velocities,

$$<P_2(\cos\Theta)> = \beta(D)/\beta(H) \quad (20)$$

From the observed numbers, Θ is 20 deg. Such a small angle suggests that the velocity of the leaving D atom is approximately parallel to that of the entering H atom, as shown schematically in Fig. 8.

The reaction of $O(^1D)$ with a hydrogen molecule is a typical example of a heavy-light-light system with a large exoergicity of 43.5 kcal mol^{-1}.[106] In this case, the photodissociation of O_2, O_3, or N_2O are convenient sources of $O(^1D)$ atoms.

$$O_3 + 266\ nm \rightarrow O(^1D) + O_2(a^1\Delta_g),$$
$$O(^1D) + HD \rightarrow HOD^{\neq} \rightarrow HO + D/\ H + OD,$$

where $HOD^{\neq}$ stands for the strongly bent intermediate state, in which the H and D atoms collide with each other within one bending oscillation. In a classical sense, when the insertion dominates, the $O(^1D)$ atom forms a complex with HD. The isotopic branching ratios of $\Phi(H+OD)/\Phi(D+OH)$ in the reaction with HD were measured. The translational energy released to the H atom $E_t(H)$ was found to be twice that released to the D atom $E_t(D)$. The measured product [H]/[D] ratio was about 1.4. In this hot and short-lived $HOD^{\neq}$ complex the H or D atom collide with each other so strongly in the very bent state that one of them leaves the hot complex as a product. Hence, $E_t(H)/E_t(D)$ becomes two due to momentum conservation between H and D during that internal collision process. Since H leaves the complex with higher probability due to its lighter mass, a [H]/[D] ratio larger than unity is explained.

Similarly, the reactions of $O(^1D)$ with HCl, Cl_2 and chlorofluorocarbons were studied.[107,108] In the reaction of HCl with $O(^1D)$, HO and $Cl(^2P_j)$ are the products. Because the H atom leaves the Cl atom with a large velocity due to its light mass, the reaction process is diabatic, resulting in the diabatic distribution in the j-branching of $Cl(^2P_j$: $j = 1/2, 3/2)$ according to Eq. 8. However, in the reaction of Cl_2 only $j = 3/2$ was produced, because ClO leaves the Cl atom with relatively small velocity and hence the adiabaticity is large in this reaction.

The reaction of an H atom with an oxygen molecule is a typical example of a light–heavy–heavy system. In this case the reaction proceeds via the complex mechanism:

$$H + O_2 \rightarrow HO_2^{\neq} \rightarrow HO + O(^3P_j)$$

The product branching ratio for the j-population in the $O(^3P_j)$ atoms is governed by the non-adiabatic interaction at the asymptotic region shown in Fig. 3, or the adiabaticity of the potential surfaces is defined by Eq. 8 in that region. The observed branching ratios were found to be rather diabatic due to the large translational energy of the H atom.[109] The reaction of a Cl atom with methane is a dominant source of HCl in the atmosphere.

The activation energy of this reaction is 2.7 kcal mol^{-1} that is close to the spin-orbit separation (2.5 kcal mol^{-1}) between $Cl(^2P_{3/2})$ and $Cl^*(^2P_{1/2})$. Thus, it was expected that the reaction rate of Cl^* would be much faster than that of Cl. In a laboratory experiment, Cl^* was produced by the 193 nm photodissociation of HCl. Because of the large adiabaticity, however, the reaction of $Cl^*(^2P_{1/2})$ with CH_4 proceeds mostly on the adiabatic potential surface that does not correlate with the two ground states, $HCl + CH_3$. Hence the reaction cross section to the $HCl + CH_3$ channel is small, while the electronic quenching of $Cl^*(^2P_{1/2})$ to $Cl(^2P_{3/2})$ occurs efficiently.[110,111]

Summary

Since Kent Wilson and Richard Bersohn first exploited the angular distribution of photofragments in the 1970s after theoretical predictions by Richard Zare, the dynamical behavior of molecules in electronically excited states has been studied extensively. The development of research in photodissociation dynamics has been accelerated by laser techniques. Kent Wilson named this mutual interaction as "Laser-in and Laser-out". Edward Teller said, "The laser has been discovered by the wrong people, namely, physicists. The result is that the chemists have not grabbed it to the extent they should. In actual fact, in every laser process, whether it starts with physics or goes through chemistry, much of it will become pure chemistry. The only people who can make real progress are the chemists". In these days his prediction has been realized. Not only do we know the mechanism of photodissociation processes, but also we visualize the structure of the molecule in the ground state and dynamical movement of atoms in the photoexcited molecule with fs lasers by Ahmed Zewail and with an imaging technique by David Chandler and Paul Houston. Even control of the excitation and dissociation has been experimentally achieved by D.S. Elliott and Robert Gordon. In the field of environmental science, research in photodissociation helps to analyze the complicated atmospheric chemistry. Future research in the field of photochemistry will be closely connected to innovative science.

M.K. thanks the Ministry of Education, Culture, Sports, Science and Technology for a grant-in-aid for Scientific Research in the priority field of "Radical Chain Reactions". R.B. thanks the U.S. Department of Energy.

References

1 R. Bersohn and S. H. Lin, *Adv. Chem. Phys.*, **55**, 1915 (1969): R. Bersohn, in "Imaging in Chemical Dynamics," A. G. Suits and R. E. Continetti, eds. American Chemical Society, Washington, DC. *ACS Symp. Ser.*, **770**, 19 (2000).

2 H. Okabe, in "Photochemistry of Small Molecules," Wiley, New York (1978).

3 "Molecular Photodissociation Dynamics," ed by M. N. R.

Ashfold, J. E. Baggott, Royal Society of Chemistry, London (1987).
4 R. Schinke, in "Photodissociation Dynamics," Cambridge University Press, Cambridge (1993).
5 B. J. Finleyson-Pitts and J. N. Pitts, Jr., in "Chemistry of the upper and lower atmosphere," Academic Press, New York (1999).
6 H. Sato, in "Photodissociation of Simple Molecules in the Gas Phase," Bunshin Publishing, Tokyo, (1992); *Chem. Rev.*, **101**, 2687 (2001).
7 A. Terenin, *Z. Phys.*, **69**, 724 (1931).
8 T. Carrington, *J. Chem. Phys.*, **41**, 2012 (1964).
9 A. Mele and H. Okabe, *J. Chem. Phys.*, **51**, 4798 (1969).
10 M. Kawasaki, Y. Hirata, and I. Tanaka, *J. Chem. Phys.*, **59**, 648 (1973).
11 N. Washida, G. Inoue, M. Suzuki, and O. Kajimoto, *Chem. Phys. Lett.*, **114**, 274 (1985).
12 H. Okabe, M. Kawasaki, and Y. Tanaka, *J. Chem. Phys.*, **73**, 6162 (1980).
13 M. Kawasaki, K. Kasatani, H. Sato, H. Shinohara, and N. Nishi, *Chem. Phys.*, **78**, 65 (1983).
14 K. Uno, T. Hikida, A. Hiraya, and K. Shobatake, *Chem. Phys. Lett.*, **166**, 475 (1990).
15 T. Ibuki, A. Hiraya, K. Shobatake, Y. Matsumi, and M. Kawasaki, *J. Chem. Phys.*, **92**, 4277 (1990).
16 K. Ohbayashi, H. Akimoto, and I. Tanaka, *Chem. Phys. Lett.*, **52**, 47 (1977).
17 L. C. Lee, *J. Chem. Phys.*, **72**, 6414 (1980).
18 S. L. Baughcum and S. R. Leone, *J. Chem. Phys.*, **72**, 6531 (1980).
19 T. Suzuki, H. Kanamori, and E. Hirota, *J. Chem. Phys.*, **94**, 6607 (1991).
20 B. Bohn, A. Doughty, G. Hancock, E. L. Moore, and C. Morrell, *Phys. Chem. Chem. Phys.*, **1**, 1833 (1999).
21 R. N. Zare, *Mol. Photochem.*, **4**,1 (1972).
22 G. E. Busch and K. R. Wilson, *J. Chem. Phys.*, **56**, 3638 (1972).
23 M. J. Dzvonik, S. C. Yang, and R. Bersohn, *J. Chem .Phys.*, **61**, 4408 (1974).
24 M. Kawasaki, S. J. Lee, and R. Bersohn, *J. Chem. Phys.*, **60**, 2647 (1977).
25 J. J. Lin, D. W. Hwang, S. Harlich, Y. T. Lee, and X.-M. Yang, *Rev. Sci. Instrum.*, **69**, 1692 (1998).
26 C. B. Moore and J. C. Weisshaar, *Annu. Rev. Phys. Chem.*, **34**, 525 (1983).
27 H. L. Berghout, S. Hsieh, and F. F. Crim, *J. Chem. Phys.*, **114**, 10835 (2001).
28 B. A. Balko, J. Zhang, and Y. T. Lee, *J. Chem. Phys.*, **97**, 935 (1992).
29 A. H. H. Chang, D. W. Hwang, X.-M. Yang, A. M. Mebel, S. H. Lin, and Y. T. Lee, *J. Chem. Phys.*, **110**, 10810 (1999).
30 J. J. Lin, C. C. Wang, Y. T. Lee, and X. Yang, *J. Chem. Phys.*, **113**, 9668 (2000).
31 D. W. Chandler and P. L. Houston, *J. Chem. Phys.*, **87**, 1445 (1987).
32 T. Sato, T. Kinugawa, T. Arikawa, M. Kawasaki, and H. Sato, *Chem. Phys.*, **165**, 173 (1992).
33 V. P. Hradil, T. Suzuki, S. A. Hewitt, P. L. Houston, and B. J. Whitaker, *J. Chem. Phys.*, **99**, 4455 (1993).
34 R. N. Dixon, *J. Chem. Phys.*, **85**, 1866 (1986).
35 C. H. Greene and R. N. Zare, *J. Chem. Phys.*, **78**, 6741 (1983).
36 P. L. Houston, *J. Phys. Chem.*, **91**, 5388 (1987).
37 G. G. Balint-Kurti and M. Shapiro, *Chem. Phys.*, **61**, 137 (1981); A. Pe'er, M. Shapiro and G. Balint-Kurti, *J. Chem. Phys.*, **110**, 11928 (1999).
38 M. N. R. Ashfold, S. G. Clement, J. D. Howe, and C. M. Western, *J. Chem. Soc., Faraday Trans.*, **89**, 1153 (1993).
39 C. A. de Lange, *Adv. Chem. Phys.*, **117**, 1 (2001).
40 S. E. van Bramer and M. V. Johnston, *Appl. Spectrosc.*, **50**, 608 (1996).
41 S. H. S. Wilson, C. L. Reed, D. H. Mordaunt, M. N. R. Ashfold, and M. Kawasaki, *Bull. Chem. Soc. Jpn.*, **69**, 71 (1996).
42 A. T. J. B. Eppink and D. H. Parker, *J. Chem. Phys.*, **109**, 4758 (1998).
43 N. Taniguchi, K. Takahashi, Y. Matsumi, S. M. Dylewski, J. D. Geiser, and P. L. Houston, *J. Chem. Phys.*, **111**, 6350 (1999).
44 R. E. Smalley, B. C. Ramakrishnan, D. H. Levy, and L. Wharton, *J. Chem. Phys.*, **61**, 4363 (1974).
45 G. E. Strauss, G. C. McBane, P. L. Houston, I. Burak, and J. W. Hepburn, *J. Chem. Phys.*, **90**, 5364 (1989).
46 P. Andresen, G. S. Ondrey, B. Titze, and E. W. Rothe, *J. Chem. Phys.*, **80**, 2548 (1984).
47 E. Segev and M. Shapiro, *J. Chem. Phys.*, **77**, 5604 (1982).
48 G. E. Hall, N. Sivakrishnan, and P. L. Houston, *J. Chem. Phys.*, **84**, 2120 (1986).
49 Y. Matsumi, K. Tonokura, and M. Kawasaki, *J. Chem. Phys.*, **97**, 1065 (1992).
50 S. J. Singer, K. F. Freed, and Y. B. Band, *Adv. Chem. Phys.*, **61**, 1 (1985).
51 E. Tiemann, H. Kanamori, and E. Hirota, *J. Chem. Phys.*, **88**, 2457 (1988).
52 J. Park, Y. Lee, and G. W. Flynn, *Chem. Phys. Lett.*, **186**, 441 (1991); **192**, 138 (1992).
53 K. Tomokura, Y. Matsumi, M. Kawasaki, S. Tasaki, and R. Bersohn, *J. Chem. Phys.*, **97**, 8210 (1992).
54 Y. Matsumi, P. K. Das, M. Kawasaki, K. Tonokura, T. Ibuki, G. Inoue, S. Satyapal, and R. Bersohn, *J. Chem. Phys.*, **97**, 5261 (1992).
55 R. Liyanage, Y. Yang, S. Hashimoto, R. J. Gordon, and R. W. Field, *J. Chem. Phys.*, **103**, 6811 (1995).
56 J. Zhang, M. Dulligan, and C. Wittig, *J. Chem. Phys.*, **107**, 1403 (1997).
57 H. M. Lambert, P. J. Dagdigian, and M. H. Alexander, *J. Chem. Phys.*, **108**, 4460 (1998).
58 D. Ascenzi, P. M. Regan, and A. J. Orr-Ewing, *Chem. Phys. Lett.*, **310**, 477 (1999).
59 P. M. Regan, S. R. Langford, D. Ascenzi, P. A. Cook, A. J. Orr-Ewing, and M. N. R. Ashfold, *Phys. Chem. Chem. Phys.*, **1**, 3247 (1999).
60 P. M. Regan, D. Ascenzi, A. Brown, G. G. Balint-Kurti, and A. J. Orr-Ewing, *J. Chem. Phys.*, **112**, 10259 (2000).
61 Ecclesiastes 1. 9.
62 M. D. Wheeler, S. M. Newman, T. Ishiwata, M. Kawasaki, and A. J. Orr-Ewing, *Chem. Phys. Lett.*, **285**, 346 (1998): M. D. Wheeler, S. M. Newman, A. J. Orr-Ewing, and M. N. R. Ashfold, *J. Chem. Soc., Faraday Trans.*, **94**, 337 (1998).
63 M. Kawasaki, H. Sato, G. Inoue, and M. Suzuki, *J. Chem. Phys.*, **91**, 6758 (1989).
64 M. Dantus, J. Rosker, and A. H. Zewail, *J. Chem. Phys.*, **87**, 2395 (1987).
65 R. Bersohn and A. H. Zewail, *Bunsen. Ges. Phys. Chem.*,

92, 373(1988).
66 M. Kawasaki, K. Kasatani, H. Sato, H. Shinohara, N. Nishi, and T. Ibuki, *J. Chem. Phys.*, **77**, 258 (1982).
67 S. K. Kim, E. R. Lovejoy, and C. E. Moore, *J. Chem. Phys.*, **102**, 3202 (1995).
68 G. W. Johnston, J. Park, S. Satyapal, N. Shafer, K. Tsukiyama, R. Bersohn, and B. Katz, *Acc. Chem. Res.*, **23**, 232 (1990).
69 M. Dzvonik, S. C. Yang, and R. Bersohn, *J. Chem. Phys.*, **56**, 3638 (1974).
70 M. Goeppert-Mayer, *Ann. Physik.*, **9**, 273 (1931).
71 M. Kawasaki and I. Tanaka, *Adv. Multiphoton Processes Spectrosc.*, **2**, 1 (1982).
72 E. A. Hinds, J. E. Clendenin, and R. Novick, *Phys. Rev. A.*, **17**, 670 (1974).
73 T. Shinzawa, A. Tokunaga, T. Ishiwata, I. Tanaka, K. Kasatani, M. Kawasaki, and H. Sato, *J. Chem. Phys.*, **80**, 5909 (1984).
74 M. Kawasaki, H. Sato, T. Kikuchi, A. Fukuroda, H. Kobayashi, and T. Arikawa, *J. Chem. Phys.*, **86**, 4425, 4431 (1987); **87**, 5722 (1987).
75 R. Vasudev, R. N. Zare, and R. N. Dixon, *Chem. Phys. Lett.*, **96**, 399 (1983); *J. Chem. Phys.*, **80**, 4863 (1983).
76 R. C. van der Wal, J. L. Scott, and F. F. Crim, *J. Chem. Phys.*, **92**, 803 (1991).
77 S. S. Brown, R. B. Metz, H. L. Berghout, and F. F. Crim, *J. Chem. Phys.*, **105**, 6293 (1996).
78 R.V. Ambartzunian and V. S. Letokhov, *Acc. Chem. Res.*, **10**, 61 (1977).
79 R. Bersohn and M. Kawasaki, *Israel J. Chem.*, **34**, 19 (1994).
80 D. J. Tannor and S. A. Rice, *Adv. Chem. Phys.*, **70**, 491 (1988).
81 I. Averbukh, M. J. J. Vrakking, D. M. Villeneuve, and A. Stolow, *Phys. Rev. Lett.*, **77**, 3518 (1996).
82 a) V. V. Yakovlev, C. J. Bardeen, J.-W. Che, J.-S. Cao, and K. R. Wilson, *J. Chem. Phys.*, **108**, 2309 (1998). b) Q.-G. Zhang, U. Marvet, and M. Dantus, *J. Chem. Phys.*, **109**, 4428 (1998).
83 M. Shapiro and P. Brumer, *Acc. Chem. Res.*, **22**, 407 (1989); *Adv. At. Mol. Opt. Phys.*, **42**, 287 (2000); R. J. Gordon and S. A. Rice, *Annu. Rev. Phys. Chem.*, **48**, 651 (1997); R. Bersohn, *J. Mol. Struct.*, **480-481**, 231 (1999).
84 a) C. Chen, Y. Y. Yin, and D. S. Elliott, *Phys. Rev. Lett.* **64**, 507 (1990); **65**, 1737 (1990). b) L-C. Zhu, K. Suto, J. A. Fiss, R. Wada, T. Seideman, and R. J. Gordon, *Phys. Rev. Lett.*, **79**, 4108 (1997); J. A. Fiss, L-C. Zhu, K. Suto, G-H. He, and R. J. Gordon, *Chem. Phys.*, **233**, 335 (1998); R. J. Gordon, L. Zhu, and T. Seideman, *J. Phys. Chem.*, **105**, 4387 (2001).
85 a) G. Q. Xing, X.B. Wang, X. Huang, R. Bersohn, and B. Katz, *J. Chem. Phys.*, **104**, 826 (1996). b) X. Wang, R. Bersohn, K. Takahashi, M. Kawasaki, and H. L. Kim, *J. Chem. Phys.*, **105**, 2992 (1996). c) H.L. Kim and R. Bersohn, *J. Chem. Phys.*, **107**, 4546 (1997).
86 R. S. Judson and H. Rabitz, *Phys. Rev. Lett.*, **68**, 1500 (1992).
87 a) A. Assion, T. Baumert, M. Bergt, T. Brixner, B. Kiefer, V. Sayfried, M. Strehle, and G. Gerber, *Science*, **282**, 919 (1998). b) R. J. Levis, G. H. Menkir, and H. Rabitz, *Science*, **292**, 709 (2001).
88 A. Iwamae, A. Hishikawa, and K. Yamanouchi, *J. Phys. B: At. Mol. Opt.*, **33**, 223 (2000).
89 H. Sakai, C. P. Safvan, J. J. Larsen, K. M. Hilligsoo, K. Hald, and H. Stapelfeldt, *J. Chem. Phys.*, **110**, 10235 (1999). J. J. Larsen, H. Sakai, C. P. Safvan, I. Went-Larsen, and H. Stapelfeldt, *J. Chem. Phy.*, **111**, 7774 (1999).
90 A. Sugita, M. Mashino, M. Kawasaki, Y. Matsumi, R. J. Gordon, and R. Bersohn, *J. Chem. Phys.*, **112**, 2164 (2000).
91 A. Sugita, M. Mashino, M. Kawasaki, Y. Matsumi, R. Bersohn, G. Trott-Kriegeskorte, and K-H. Gericke, *J. Chem. Phys.*, **112**, 7095 (2000).
92 J. J. Larsen, I. Wendt-Larsen, and H. Stapelfeldt, *Phys. Rev. Lett.*, **83**, 1123 (1999).
93 A. Sugita, K. Suto, M. Kawasaki, and Y. Masumi, *Chem. Phys. Lett.*, **340**, 83 (2001).
94 T. Suzuki, H. Takayanagi, S. Nanbu, and M. Aoyagi, *J. Chem. Phys.*, **109**, 5778 (1998).
95 C. D. Pibel, K. Ohde, and K. Yamanouchi, *J. Chem. Phys.*, **101**, 836 (1994).
96 P. C. Samartzis, B. L. Bakker, T. P. Rakitzis, and D. H. Parker, *J. Chem. Phys.*, **110**, 5201 (1999).
97 K. Takahashi, M. Kishigami, N. Taniguchi, Y. Matsumi, M. Kawasaki, and A. J. Orr-Ewing, *J. Chem. Phys.*, **105**, 5920 (1996); K. Takahashi, M. Kishigami, Y. Matsumi, M. Kawasaki, and M. N. R. Ashfold, *J. Chem. Phys.*, **108**, 7161 (1998).
98 A. Ravishankara, G. Hancock, M. Kawasaki, and Y. Matsumi, *Science*, **280**, 60 (1998); Y. Matsumi, F. J. Comes, G. Hancock, A. Hofzumahaus, A. J. Hynes, M. Kawasaki and A. R. Ravishankara, *J. Geophy. Res.*, **107** (D3), 10.1029/2001 JD 00510 (2002).
99 Y. Matsumi, S. M. Shamsuddin, Y. Sato, and M. Kawasaki, *J. Chem. Phys.*, **101**, 9610 (1994).
100 Y. Matsumi and A. M. S. Chowdhury, *J. Chem. Phys.*, **104**, 7036 (1996).
101 R. K. Talukdar, C. A. Longfellow, M. K. Gilles, and A. R. Ravishankara, *Geophys. Res. Lett.*, **25**, 143 (1998).
102 W. Denzer, G. Hancock, J. C. Pinot de Moira, and P. L. Tyley, *Chem. Phys.*, **231**, 109 (1998).
103 K.-P. Liu, *Ann. Rev. Phys. Chem.*, **52**, 139 (2001); *Internat. Rev. Phys. Chem.*, **20**, 189 (2001).
104 M. Kawasaki, *J. Photochem. Photobiol. A*, **106**, 105 (1997).
105 A. Chattopadhyay, S. Tasaki, R. Bersohn, and M. Kawasaki, *J. Chem. Phys.*, **95**, 1033 (1991).
106 Y. Matsumi, K. Tonokura, M. Kawasaki, and H. L. Kim, *J. Phys. Chem.*, **96**, 10622 (1992).
107 Y. Matsumi, K. Tonokura, M. Kawasaki, K. Tsuji, and K. Obi, *J. Chem. Phys.*, **98**, 8330 (1993).
108 M. Kono and Y. Matsumi, *J. Phys. Chem. A*, **105**, 65 (2001).
109 Y. Matsumi, N. Shafer, K. Tonokura, M. Kawasaki, and H. L. Kim, *J. Chem. Phys.*, **95**, 4972 (1991).
110 Y. Matsumi, K. Izumi, V. Skorokhodov, M. Kawasaki, and N. Tanaka, *J. Phys. Chem. A*, **101**, 1216 (1997).
111 K. Hitsuda, K. Takahashi, Y. Matsumi, and T. J. Wallington, *J. Phys. Chem. A*, **105**, 5131 (2001).

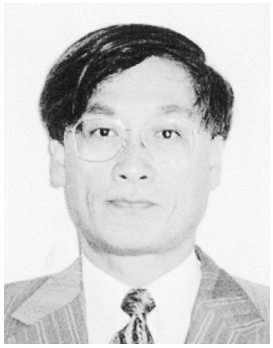

Masahiro Kawasaki was born in 1947 in Shiga, Japan. He received his B. Eng. in 1969 and M. Eng. in 1971 from Kyoto University, and D. Sci. (Thesis supervisor, I. Tanaka) in 1974 from Tokyo Institute of Technology. After he worked in Research Lab, Mitsubishi Oil Company, he was appointed to be research associate at Department of Chemistry, Columbia University with R. Bersohn in 1974, research associate at Department of Chemistry, Tokyo Institute of Technology in 1976, associate professor at Department of Chemistry, Mi'e University in 1979, professor at Institute for Electronics Sciences and Graduate School of Environmental Earth Sciences, Hokkaido University in 1987. Since 1997, he has been professor at Department of Molecular Engineering, Kyoto University and adjunct professor of Graduate School of Global Environment Studies, Kyoto University. His research interest is photodissociation dynamics of small molecules, and environmental atmospheric chemistry. Awards: Inoue Science Award (1994), Japan Photochemical Society Award (1994).

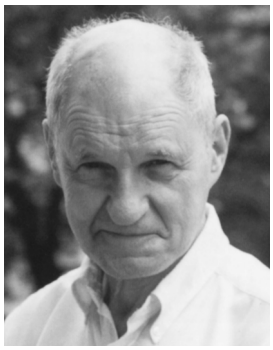

Richard Bersohn, Born in New York City, U. S. A. in 1925. B.S. in Chemistry, MIT in 1943, M.A. in Physics, Harvard in 1947, Ph.D. Harvard in 1950 (Thesis supervisor, J.H. van Vleck), Postdoctoral fellow at Columbia 1949 with Willis Lamb, Associate Professor of Cornell University in 1951. Since 1959, He has been professor at Department of Chemistry, Columbia University and now the Higgins Distinguished Professor of Natural Science, Columbia University. Member of editorial boards of Chemical Reviews, Journal of Physical Chemistry, Israel Journal of Chemistry, Journal of Chemical Physics, Physical Review Letters, Chemical Physics, Chemical Physics Letters. Head of Division of Chemical Physics of American Physical Society in 1971, Advisory Committee to Brookhaven National Laboratory for 1981–1984, Committee on Atomic and Moleculrar Science of the National Research Council for 1984–1987, Membership: American Academy of Arts and Sciences, National Academy of Sciences. Award: H. Broida prize in chemical physics (American Physical Society, 1985)